

# SEA WAVE PATTERN EVALUATION

Part 2 Report: Investigation of Accuracy

E.O. Tuck, D.C. Scullen and L. Lazauskas

Applied Mathematics Department  
The University of Adelaide

31 May 1999

## Abstract

Flow about a spheroid submerged beneath a free surface is considered in order to determine the ability of thin-ship theory and its implementation in the computer program *SWPE* to reproduce the free-surface shape accurately. A verification code is utilised, and comparisons are made between a fully-nonlinear representation, a linearised free-surface boundary condition representation, and the thin-ship representation of this code. This comparison allows us to determine, in a systematic manner, the source and magnitude of any inaccuracies that are found. Finally, the results produced by the verification code are compared with those produced by *SWPE*, in order to establish the accuracy of the *SWPE* code.

---

The front cover of this report is a far-field contour plot of wave elevations for a spheroid which is 100m long and 10m in diameter, submerged to a depth such that there is one diameter clearance between its top and the free surface, travelling at a Froude number of 0.8, i.e. a speed of  $25\text{ms}^{-1}$  or 49 knots. The plot was constructed using *SWPE* with a high resolution of 300 grid points in each direction, over a domain extending from 590m to 2090m downstream of the centre of the body, and 750m either side of the track. The highest elevations shown (whitest domains) are of the order of one metre.

# 1 Introduction

This report investigates the accuracy of the Sea-Wave-Pattern-Evaluation program (SWPE) described in the Part 1 report [5]. The present investigation can be broken into two main parts — that which deals with the consistency and accuracy of various implementations of the verification code, and that which compares the thin-ship implementation of the verification code with the results produced by the much faster SWPE code.

The first part of the investigation is intended to show in which circumstances the thin-ship theory is an appropriate approximation for flows about a submerged spheroid, and the error that is likely to be introduced by the thin-ship approximations. There are two mathematical simplifications that are made by thin-ship theory. The major simplification is that which is common to all linear theories — namely that the kinematic and dynamic free-surface boundary conditions can be approximated by a linearised condition on the plane equilibrium surface. The second simplification is that the disturbance to the flow that is created by the body can be approximated by a (known) continuous distribution of singularities along the centre-plane of the thin body. To gain a better understanding of the influence that these two distinct simplifications have on the accuracy of the approximation, it is necessary to consider their numerical consequences separately. In order to do this, a verification code developed by Scullen [2] which is capable of reproducing the different combinations of approximations will be utilised.

Three implementations of the verification code will be used. The “*nonlinear mode*” enforces the exact Neumann boundary condition on the body, and both the kinematic and dynamic exact (“Stokes”) boundary conditions on the actual displaced free surface. The “*linear mode*” also enforces the exact Neumann boundary condition on the body, but approximates the free surface by enforcing the linearised (“Kelvin”) boundary condition on the plane  $z = 0$ . Finally, the “*thin-ship mode*” uses the approximate Kelvin free-surface condition and in addition approximates the body boundary condition by use of a continuous distribution of singularities of predetermined (“Michell”) magnitude along the centre-plane.

Investigations are made to establish that these implementations are consistent with each other and with the result that was obtained from slender-body theory by Havelock [1]. The assumption will then be made that the nonlinear mode renders, of the three modes, the best approximation to the (unknown) exact solution, and the nonlinear-mode results will be used as the basis for comparison in determining the accuracy of the thin-ship mode.

Two error measures are used, one of which identifies maximum errors, oc-

curing at the highest crests in the wave field. Such local isolated errors can be as high as the order of 50% for the most shallow submergences used where the highest waves are near to breaking, but reduce dramatically as the submergence is increased. However, the general magnitude of the error in the whole wave field is only of the order of 5% or less, and this is displayed by use of a root-mean-square error estimate. As the submergence is increased, the errors do not reduce to zero, but there is a small (2% to 3%) residual error attributable to the inability of the thin-ship theory to capture the true local flow around the nose and tail of bluff bodies such as spheroids.

The second part of the investigation will show the magnitude of the errors that exist when using SWPE, by giving a direct comparison of the results produced by that program with those produced by the verification program in both nonlinear and thin-ship modes. It will be shown that there is, in general, very good agreement between SWPE and the verification program in thin-ship mode.

## **2 Accuracy of the Thin-Ship Theory**

### **2.1 Establishment of the accuracy of the verification code**

Before proceeding to compare the SWPE code with the verification code, it is necessary to establish that the verification code does indeed give accurate solutions for potential flow about a submerged body. Unfortunately, there is no easy way in which to do this, since no closed-form expressions for the solution to the exact nonlinear problem are available. There is, however, one analytic expression available for the linearised free-surface problem from slender-body theory.

It is possible to show that the verification code in linear mode produces accurate solutions to the linearised problem, and to infer from this that the verification code in nonlinear mode produces accurate solutions to the nonlinear problem. The validity of this approach was authenticated by Scullen and Tuck [3] where the nonlinear mode was compared with both the standard linear theory and an enhanced second-order linear theory for flow over submerged circular cylinders (Tuck [4]).

So, as a preliminary to the main investigation, it is first necessary to establish that the verification code is accurate in its most basic form, the linear mode. In this mode, the Neumann boundary condition is satisfied on the body, and the linearised free-surface condition is satisfied over the plane surface  $z = 0$ , each at a collection of collocation points. The potential is represented by a distribution of source singularities external to the flow field, whose strengths are determined by

the program. More specific details of the method are described in [2].

Dimensional analysis shows that all cases of interest here can be described by just three dimensionless parameters — the diameter-to-length ratio of the spheroid, the diameter-to-depth ratio, and a length-based Froude number.

Two spheroid shapes, one with a diameter-to-length ratio of 1:10 and the other with a diameter-to-length ratio of 1:8 are considered.

Diameter-to-depth ratios varying from 0.1 (deeply submerged) to 1.0 (shallowly submerged) are considered. The “depth” is measured here from the centre-line of the spheroid up to the free surface plane.

For a spheroid of length 100 metres, with acceleration due to gravity of approximately 9.81 metres per second per second, a Froude number of 0.3 corresponds to a speed of approximately 34 kilometres per hour or 18 knots, and a Froude number of 1.0 corresponds to a speed of approximately 113 kilometres per hour or 61 knots. Thus, Froude numbers in the range of 0.3 to 1.0 are of interest here.

Firstly, an accurate representation of the flow about a spheroid is sought, such that the flux through the body’s surface is minimal. On the basis of the investigation, one particular representation is preferred. This representation uses 65 stations, each (except the points at the actual nose and tail) having 32 nodes equally spaced in angle around the circumference of the circular cross-section. However, due to lateral symmetry, the domain of interest may be halved, so that the actual representation which is implemented uses 65 stations of 17 nodes equally spaced over one half of the spheroid, each with an associated image.

Similarly, a representation of the free surface which simultaneously satisfies several criteria is sought. The free-surface domain must extend far enough downstream to capture several wavelengths, far enough upstream to implement a radiation condition, be large enough to represent the flow around the body, have fine enough resolution to resolve both the free-surface waves and the body, and be comprised of few enough collocation points to be computationally feasible. Needless to say, it is not always possible to satisfy all of the criteria given current super-computing capabilities, especially at the more extreme high and low values of Froude number. Nevertheless, one representation which uses 91 collocation points in the  $x$ -direction, 25 collocation points in the  $y$ -direction and extends from  $-3.75U\sqrt{L/g}$  to  $7.5U\sqrt{L/g}$  proves to be adequate over the range of Froude numbers that are considered here. Here as in the previous report, the vessel is translating in the negative  $x$ -direction, with the  $y$ -direction to port, and  $z$  increasing upwards. The speed of the vessel is  $U$ ,  $L$  is the spheroid’s length and  $g$  is acceleration due to gravity.

Having found suitable representations of the body and free-surface, it is necessary to establish the accuracy of the code when using these representations. To do this, the code is implemented in linear mode which, as mentioned above, makes the assumption of a linearised free-surface boundary condition. For comparison with Havelock's slender-body theory, the wave resistance of the body is determined. The results for the 1:10 spheroid are shown in Figure 1 where the wave resistance  $R$  has been scaled with respect to the spheroid's buoyancy, and it is the dimensionless wave resistance

$$\bar{R} = \frac{R}{\frac{1}{6}\pi\rho g L d^2} \quad (1)$$

which has been plotted. Here,  $\rho$  represents the fluid's density,  $d$  the spheroid's diameter and, in reference to the figures,  $d/f$  represents the diameter-to-depth ratio. The error in the wave resistance is very small at all Froude numbers and diameter-to-depth ratios, indicating that the representation of the body and free surface is accurate. The results for the 1:8 spheroid have similar characteristics.

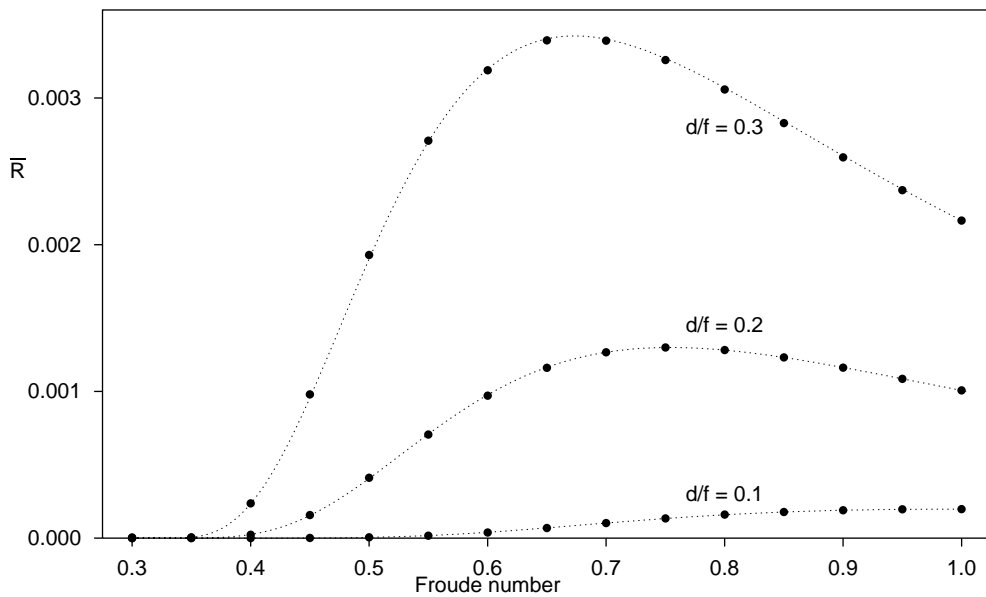


Figure 1: Wave resistance of the 1:10 spheroid as determined by the verification code in linear-mode (large dots), compared with that which can be expected from Havelock's slender-body theory (dotted curves).

Having established the accuracy of the verification code in linear mode, it is

now acceptable to introduce the nonlinear free-surface boundary conditions. The code is run in nonlinear mode, for the same cases as described above.

For sufficiently small values of the diameter-to-depth ratio (that is, for sufficiently deep spheroids) the results are of course consistent with those produced in linear mode. Naturally, for larger values of this parameter (that is, shallower spheroids) the nonlinear effects become noticeable. Without further justification (other than that offered in [3]) it will be assumed that the results produced by the nonlinear implementation are an accurate solution to the flow for the fully-nonlinear problem.

## 2.2 Thin-ship computations

As already noted, the thin-ship theory makes two assumptions — one being that a linearised free-surface boundary condition is implemented, and the other being that the thin body is accurately represented by a continuous distribution of sources placed along the centre-plane and of strength given in terms of the body geometry by the Michell formula  $\sigma = 2Uf_x(x, z)$ , where  $y = \pm f(x, z)$  is the body's surface.

A thorough investigation of the accuracy of the thin-ship theory must include both direct comparison of the thin-ship results with the nonlinear results and a breakdown showing the components of the error that may be attributed to the violation of each of the two thin-ship-theory assumptions. We take this approach here, giving first a measure of the discrepancy between the thin-ship-mode results and the nonlinear-mode results, and then a measure of the discrepancy between the thin-ship-mode results and the linear-mode results. The former will show the total error, and the latter will show that which is due to inaccuracies in the body representation (the difference between them being due predominantly to the linearised free-surface assumption).

It can easily be shown (by integrating by parts) that the distribution of source singularities of interest here is equivalent to a continuous distribution of dipoles of moment  $\mu = 2Uf(x, z)$ , provided that  $f(x, z) = 0$  on the perimeter of the region. In the context of thin-ship theory, the region of concern is the projection of the body surface onto the centre-plane and, for many hulls of interest (and in particular for spheroids),  $f(x, z) = 0$  on the perimeter of this region. Thus, it is equivalent to represent the body by a continuous distribution along the centre-plane of dipoles (aligned in the  $x$ -direction) of moment  $\mu = 2Uf(x, z)$  proportional to the local width of the body.

It is not possible to write a closed-form solution for the potential at a point due to a continuous distribution of either sources or dipoles as described above,

and therefore the continuous distribution must be approximated by a collection of discrete sources or dipoles, with strengths or moments weighted further by the area that they represent. In essence, the integration must be performed by quadrature.

The substitution of sources for dipoles has two immediate and numerically-significant implications. Most importantly, it avoids the problem of numerically integrating a function which would otherwise be singular at every point along the boundary of the centre-plane of the spheroid. The second advantage is that not only is the integrand finite on  $y = 0$  but it is zero, allowing a little less care to be taken when discretising the region of integration. (A rectangular discretisation of the centre-plane would normally have to be concerned with the area of panels that overlap the boundaries of the region of integration — not so if the integrand is zero there.)

The representation of the spheroid that is used here discretises the ellipse into a series of vertical stations, each broken into an equal number of rectangular cells. Trapezoidal-rule weights are used, so that singularities can be placed on the actual boundary of the projection, rather than just away from it.

It seems unlikely, given the speed of the SWPE code, that much attention will be given in use of that code to optimisation of the representation of the body, with improvements in accuracy being obtained simply by increasing the resolution. No optimisation of the discretisation is attempted here for the verification code in thin-ship mode either. Rather, a number of points that is consistent with that for the nonlinear-mode representation is used in the representation. In this case 65 stations are used, each with 17 dipoles.

Comparisons between the two surfaces produced by the verification code in nonlinear mode and thin-ship mode are made for both the 1:8 and 1:10 spheroids, over the range of diameter-to-depth ratios and Froude numbers described above. For each pair of free surfaces, error measures are calculated using the nonlinear mode's result as the basis for the comparison. In particular, a scaled range and a scaled root-mean-square (rms) error are determined. The method for calculating these measures is as follows.

We determine both the maximum and minimum elevations of the free surface produced in nonlinear mode. The difference between these two values is a measure of the magnitude of the disturbance produced by the body, and will be used to scale the absolute errors, so that comparisons of errors in free surfaces produced for other cases of Froude number and diameter-to-depth ratio can be made. We call this value the *free-surface range* for the nonlinear free surface.

At each point on the free surface, determine the difference between the thin-

ship mode's elevation and the nonlinear mode's elevation. This is the *free-surface error*.

We determine both the maximum and minimum elevations of the free-surface error. The difference between these maximum and minimum values is a measure of the magnitude of the error in the free surface. We call it the *error range* of the free-surface.

The ratio between the error range and the surface range of the nonlinear free surface is a dimensionless quantity which can be used for comparison with other cases. It can be thought of as a measure of the relative error in the thin-ship mode's free surface. We call this value the *relative error range* of the free surface.

In a similar manner, we can determine the rms error in the free-surface, and divide it by the range of the free-surface. This too is a dimensionless quantity which can be thought of as an alternative measure of the relative error in determination of the thin-ship mode's free surface. We call it the *relative rms error* in the free surface.

The error range of the free-surface is an upper bound for the correction that needs to be made to the thin-ship mode's free surface, and tends to overstate the discrepancies at points of the surface other than that where the maximum error occurs. It is entirely determined by errors that occur at very highest crest and deepest trough in the wave field (usually in the near field close to the stern), and in particular the highest crest can be close to or actually breaking when the body is shallowly submerged. It is difficult for any numerical code to estimate such near-breaking crests, and differences between various estimation methods, including the linear and thin-ship modes tested here, become exaggerated. Meanwhile, however, at points other than the extreme crests and troughs, the errors are far less at the same speeds and submergences.

This is accounted for by the rms error, which averages errors over the whole flow field. On the other hand, the rms error slightly understates the magnitude of the error, since a significant part of the domain where computations are being compared lies upstream of the wake, where disturbances are small and hence small contributions are made to the average. However, a combination of these two measures of the error can be useful to judge the accuracy of the results.

Figure 2 shows the relative error range for the 1:8 spheroid for the standard cases of Froude number and diameter-to-depth ratio, while Figure 3 shows the relative rms error for the same cases. The diameter-to-depth ratio increases in steps of 0.1 from bottom to top in this and other curves in this series. That is, the bottom curve is for diameter-to-depth ratio 0.1 with the largest submergence, while the top curve has diameter-to-depth ratio 1.0 and is shallowly submerged.

The relative error range in the latter case is large, of the order of 50% or more, but this is the phenomenon described above where the highest crest is so large that it is on the verge of breaking and is inevitably poorly predicted by the linear and thin-ship assumptions. On the other hand, the lowest curve in the figure, for diameter-to-depth ratio 0.1, for deeply submerged bodies, has relative error ranges of the order of 4% or less, and is much reduced because the waves are smaller and more easily predicted.

Meanwhile, the rms error as displayed in Figure 3 is consistently much lower than the relative error range, of the order of 5% for shallowly-submerged bodies at low Froude number, reducing to the order of 2% or less for all submergences at high Froude number.

Similarly, Figures 4 and 5 show the relative error range and relative rms errors for the 1:10 spheroid respectively. These errors are less than those for the 1:8 spheroid as we should expect for a more slender body making *smaller* waves at fixed submergence depth. However, it should be pointed out that at fixed diameter-to-depth ratio, the 1:10 spheroid is more shallowly submerged, which would (if it were not for the reduced slenderness) make for *larger* waves. These two effects in part cancel each other out, and the differences in errors between the 1:10 and 1:8 spheroids (at fixed diameter-to-depth ratio) are not as great as might be expected.

These four figures give an indication of the total error that is to be expected when approximating the nonlinear formulation by the thin-ship formulation. Of particular interest is the fact that the errors tend to a non-zero minimum as the diameter-to-depth ratio is decreased; that is, as the body becomes more and more deeply submerged. This indicates that there is a residual error associated with the thin-ship approximation to the body boundary condition, independent of the free surface.

To determine which component of this error is due to the approximation of the body boundary condition, it is necessary to repeat these comparisons, again using the thin-ship-mode results as the approximation, but this time using the linear results as the basis for the comparison.

Figures 6–9 show the relative error range and rms errors for both the 1:8 and 1:10 spheroids, when the thin-ship-mode result is compared to the linear-mode free surface. The large errors in the highest crests for shallowly-submerged bodies (in the top curves for which the diameter-to-depth ratio is 1.0) exhibited by the relative-error-range graphs are now significantly reduced, indicating that nonlinear free-surface effects account for much (but not all) of this error.

On the other hand, one can see that the error does not tend to zero as the diameter-to-depth ratio approaches zero, and the residual error in this limit is not

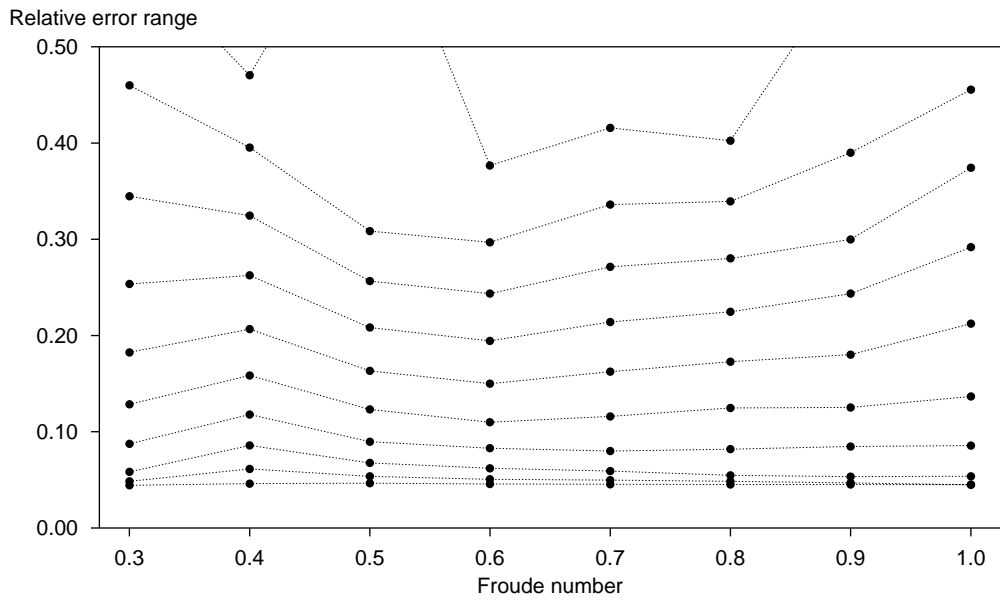


Figure 2: Relative error range in the free surface produced by the thin-ship mode when compared to that produced by the nonlinear mode for the 1:8 spheroid. In this and other figures to follow the diameter-to-depth ratio increases in steps of 0.1, from 0.1 to 1.0 from bottom curve to top curve.

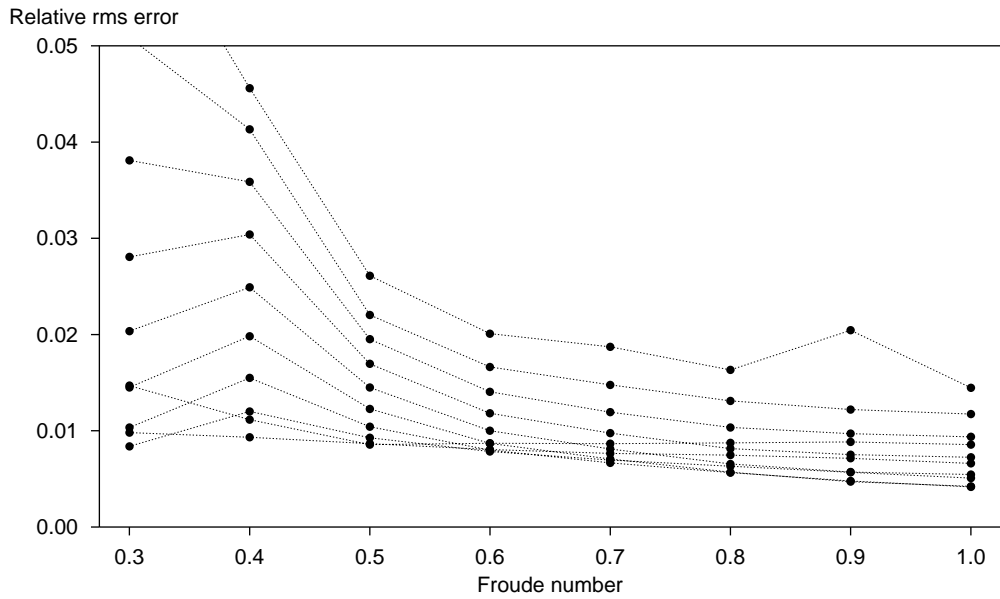


Figure 3: Relative rms error in the free surface produced by thin-ship mode when compared to that produced by nonlinear mode for the 1:8 spheroid.

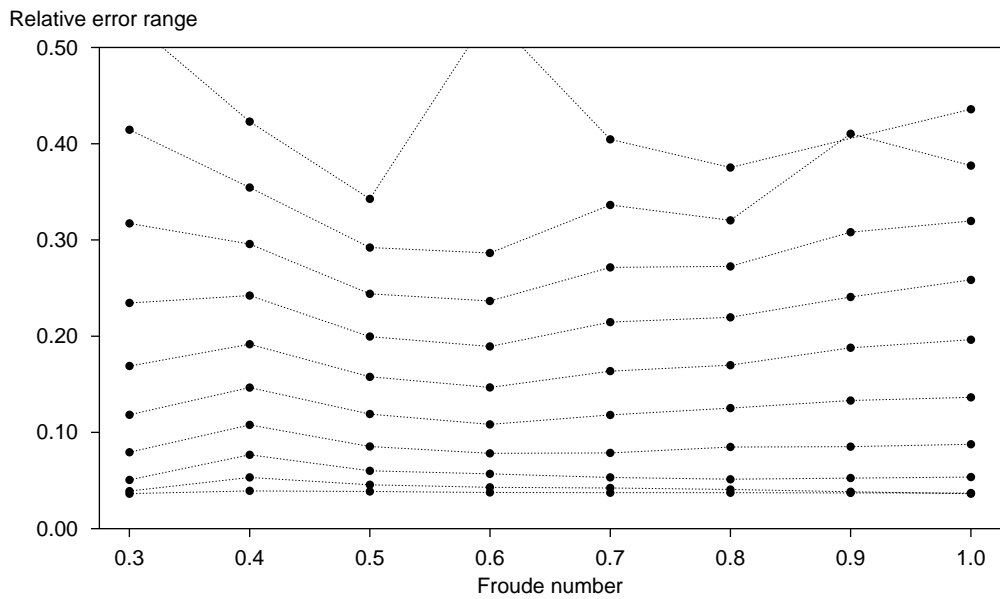


Figure 4: Relative error range in the free surface produced by the thin-ship mode when compared to that produced by the nonlinear mode for the 1:10 spheroid.

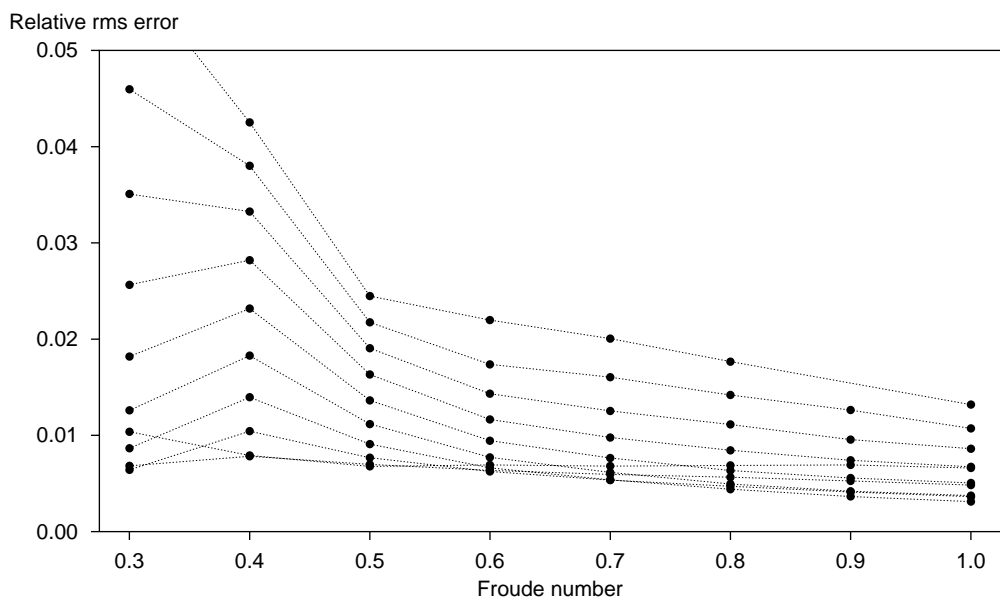


Figure 5: Relative rms error in the free surface produced by the thin-ship mode when compared to that produced by the nonlinear mode for the 1:10 spheroid.

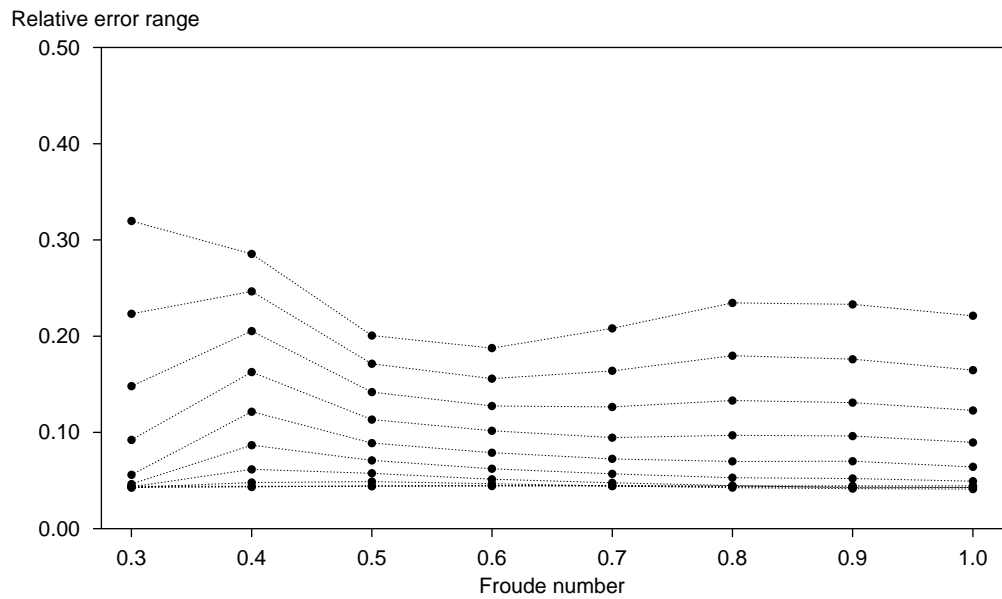


Figure 6: Relative error range in the free surface when the thin-ship mode results are compared to the linear-mode results for the 1:8 spheroid.

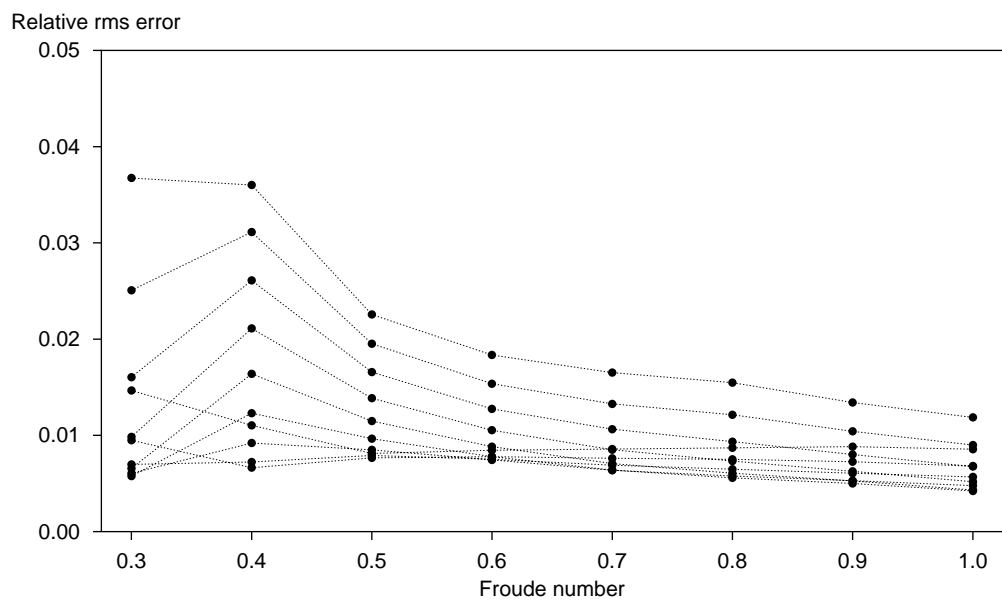


Figure 7: Relative rms error in the free surface when the thin-ship mode results are compared to the linear-mode results for the 1:8 spheroid.

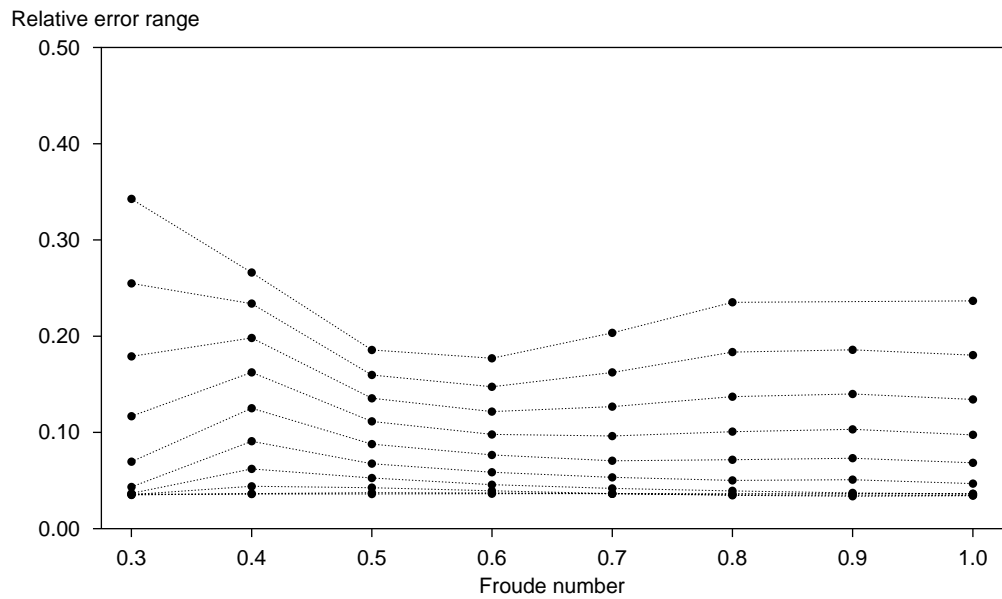


Figure 8: Relative error range in the free surface when the thin-ship mode results are compared to the linear-mode results for the 1:10 spheroid.

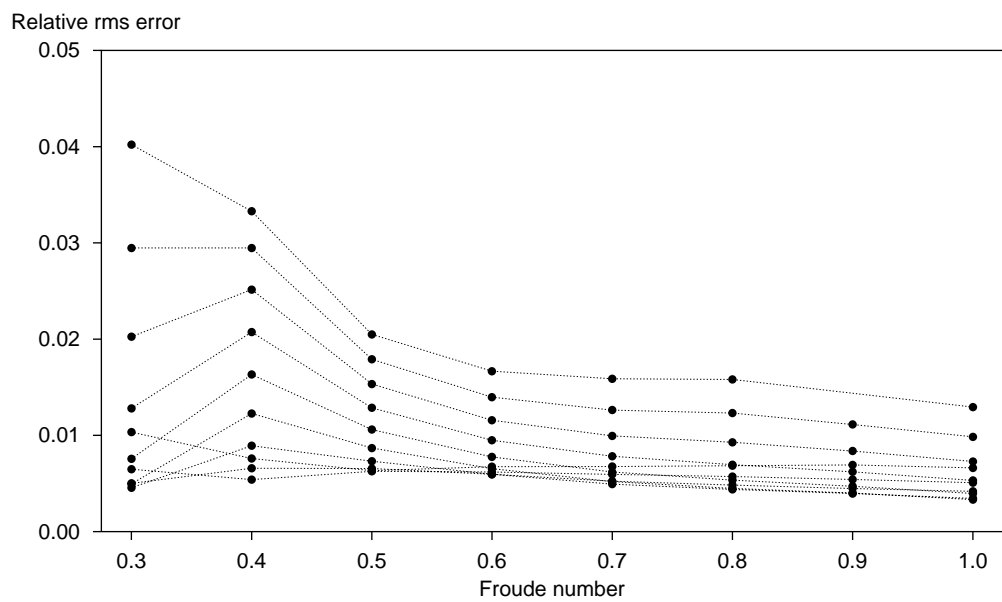


Figure 9: Relative rms error in the free surface when the thin-ship mode results are compared to the linear-mode results for the 1:10 spheroid.

significantly reduced from those relative to the nonlinear mode. The residual errors of the order of 3% for deeply-submerged bodies are thus due to the inability of the distribution of singularities along the centre-plane to reproduce the flow about the body in an accurate manner. Such 3% errors will be present at all depths, though overwhelmed by larger free-surface errors for shallow submergences.

A similar test has been done comparing the linear-mode and nonlinear-mode free surfaces. Although the results are not shown here, the error then does tend to zero as the diameter-to-depth ratio tends to zero, as expected. All errors in this case are now due to the approximation made by use of the linearised free-surface condition.

As an aside, one should note that the effects of the two approximations are not simply additive. That is, one cannot simply take the error due to nonlinearity and add it to the error due to the body's representation, and arrive at the error in the thin-ship approximation. It appears that sum of the errors due to the individual effects is greater than the error due to both approximations.

The conclusion to be drawn is that the residual error seen in the figures for the thin-ship mode is due entirely to the inaccurate representation of the body by the thin-ship theory. This source of error will be investigated in the next section.

### **2.3 Thin-ship body representation**

The conclusion that the body boundary condition approximation produces a residual error is supported further when we analyse the wave resistance produced by the various formulations, again using the nonlinear results as the basis for comparison. Although we do not show the results here, we see a similar pattern, with the error in the linear-mode results tending to zero as the diameter-to-depth ratio is decreased, but the error in the thin-ship-mode results tending to a non-zero limit. For the 1:8 spheroid, this limiting error is approximately 8%, and for the 1:10 spheroid it is 6%.

We now investigate the cause of this residual error more fully, by a detailed examination of the flow field close to the body surface. In particular, we determine the component of the fluid's velocity that is normal to the body's surface at a collection of points on that surface, when it is immersed in an uniform stream without a free surface. For comparison, we do this for both the nonlinear mode's body representation (which satisfies the Neumann boundary condition exactly at a collection of specified collocation points) and the thin-ship mode's body representations. For the nonlinear mode (which, in the absence of a free surface, is identical to the linear mode), the collection of points at which the normal velocity

is determined is found by using twice the resolution (approximately 4 times as many nodes) that was used to determine the original collocation points. In the thin-ship mode, the collocation points are determined by doubling the resolution used to produce the singularity locations, and then projecting (in the  $y$ -direction) these locations onto the body's surface.

Figure 10 shows the value of the inward normal velocity  $\partial\phi/\partial n(x, z)$  over the 1:10 spheroid's surface, when the code is in nonlinear mode. Note that the centre-plane of the plot is being viewed from slightly above, behind and to port. A *positive* value of  $\partial\phi/\partial n(x, z)$  represents flow *into* the body. Note that the maximum error at these points is less than 1% of the uniform-stream's velocity (its average is 0.05%). Figure 11 shows the same plot, but viewed from directly above the spheroid. One can see clearly that the maximum errors occur at the leading and trailing edges, where the body is bluff. In principle, the magnitude of these errors can be reduced to zero everywhere as the resolution of the body is enhanced.

By comparison, Figure 12 shows the normal velocity when the code is in thin-ship mode. Note that the maximum error at these points is almost three times the uniform-stream's velocity, and the average is 13%. Figure 13 shows the results when viewed from directly above the spheroid. Again the maximum errors occur at the bow and stern where the body is bluff and the thin-ship assumption is violated. The few points of larger error are a result of discretisation of the body, and these errors could be reduced by increasing the resolution of the body representation. However, one can also see a clear and underlying pattern which extends the entire length of the body. These errors are a direct result of the thin-ship approximation, and cannot be reduced by an increase in resolution of the body's representation. Their magnitude alone is much greater than that which is present in the nonlinear-mode results.

The figure shows that there is an influx of fluid at the leading edge and an outflow at the trailing edge, the net effect of which is to under-represent the disturbance that should be created by the body. In the presence of a free surface, this results in both smaller wave amplitude and wave resistance than the correct value and therefore explains the discrepancy found earlier in the thin-ship results. One important point is that this effect will occur whether or not there is a free surface, and therefore cannot be eliminated as diameter-to-depth ratio is decreased. The only thing that can be done to improve the situation is to choose the strengths (and locations) of the singularities that represent the body in such a way that the Neumann boundary condition is satisfied better — however, the thin-ship body boundary condition approximation precludes this to a large extent.

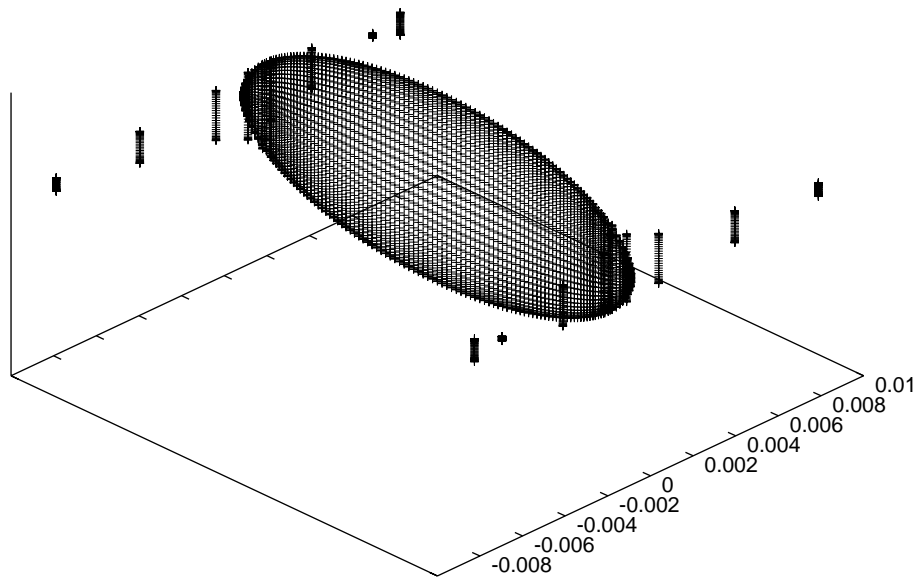


Figure 10: Velocity of flow through the surface at various points on the body when represented in nonlinear mode. The centre-plane is viewed from above, behind and to port.

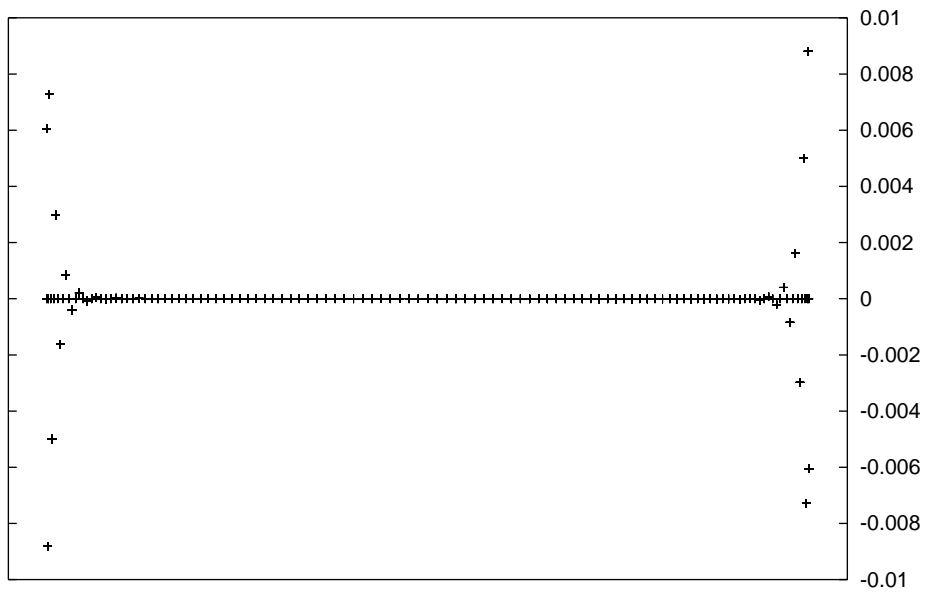


Figure 11: Velocity of flow through the surface at various points on the body when represented in nonlinear mode. The centre-plane is viewed from directly above.

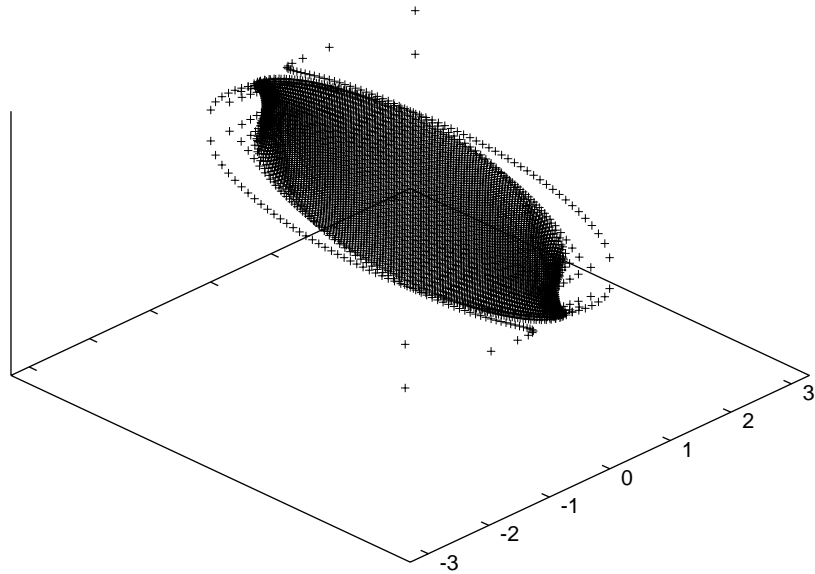


Figure 12: Velocity of flow through the surface at various points on the body when represented in thin-ship mode. The centre-plane is viewed from above, behind and to port.

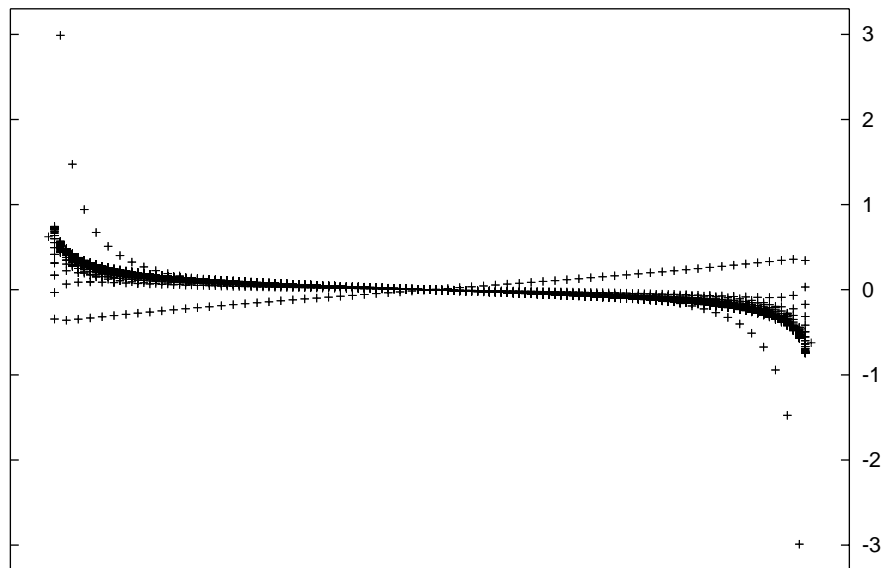


Figure 13: Velocity of flow through the surface at various points on the body when represented in thin-ship mode. The centre-plane is viewed from directly above.

### 3 Comparison of results with SWPE

To determine the accuracy of the SWPE code, we are interested in the comparison of the free surfaces produced by both the thin-ship codes. To this end, the SWPE code is run using a diameter-to-depth ratio of  $2/3$  (so that the top of the spheroid is exactly one diameter deep) over the range of Froude numbers and for the two diameter-to-length-ratio spheroids considered above.

Figure 14 shows the relative range of the free-surface error for the three cases of the verification code in linear mode, the verification code in thin-ship mode, and the SWPE code, and Figure 15 shows the relative rms error in the free surface, both for the 1:8 spheroid. Note that the domain of comparison contains only the last 49 rows of collocation points of the verification code's domain (which contains 89 rows in the free-surface) since to compare further upstream is unfair to SWPE as it is currently implemented for the far field only (the first 29 rows lie upstream of the body's centre). Similarly, it is computationally prohibitive for the verification code's domain to extend further downstream. Nevertheless, the domain of comparison is adequate. Similarly, Figures 16 and 17 show the relative range and rms errors for the 1:10 spheroid. We expect that the SWPE code could perform better than the verification code, if it were to use a high-enough resolution over the body's centre-plane distribution.

As one could expect from the previous observations, the linear-mode results show the smallest differences from SWPE and these differences tend to zero as the diameter-to-depth ratio decreases (that is, where the nonlinear nature of the free surface becomes negligible). The thin-ship-mode results had already showed that there is a contribution to the error that is due to the inability of the thin-ship theory to capture the actual flow about the body. The results produced by SWPE fare slightly worse, the additional errors being due mostly to absence of a near-field component in its current implementation. Additional sources of error include the fact that the SWPE results are produced with a slightly different representation of the body which does not capture the flow at the bow and stern as accurately as does the thin-ship implementation in the verification code, and that there is some error in the verification code's results at high Froude number (as will be discussed soon).

Figures 18–21 show the relative errors for the 1:10 spheroid at Froude numbers 0.4, 0.6, 0.8 and 1.0 respectively. The lower half of the plot shows the relative error inherent in the verification code's thin-ship mode, and the upper half shows the relative error in the SWPE code, both when compared to the verification code in its most accurate nonlinear mode. In each instance, the results are scaled so that

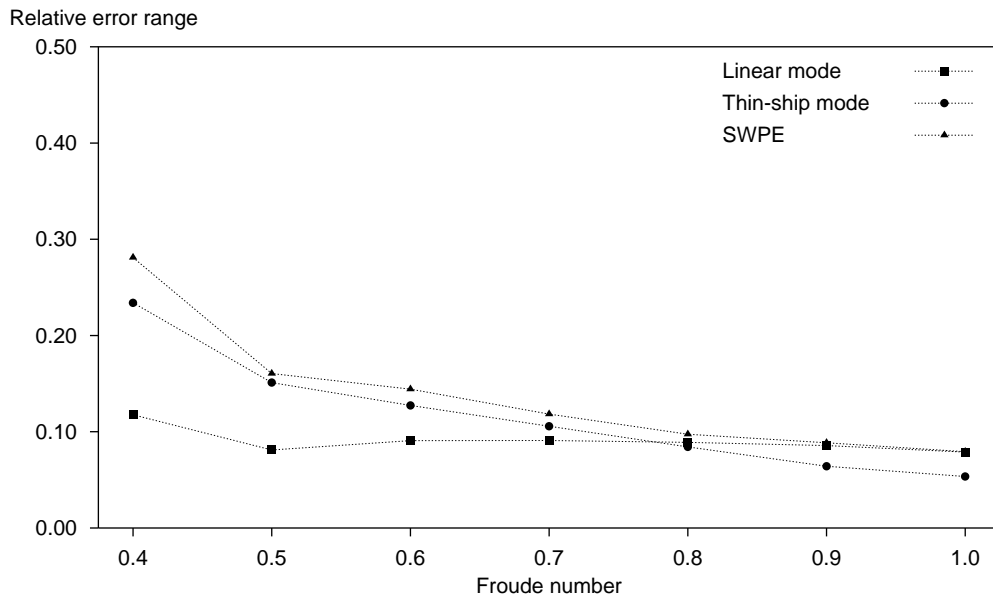


Figure 14: Relative error range in the free surface as produced by linear mode, thin-ship mode and SWPE when compared with nonlinear-mode results for the 1:8 spheroid.

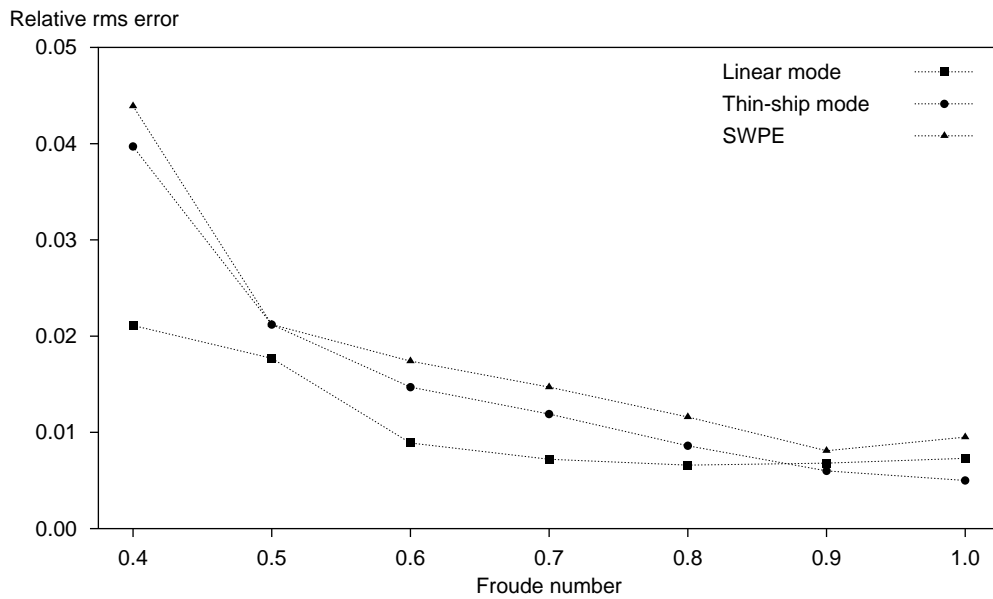


Figure 15: Relative rms error in the free surface as produced by linear mode, thin-ship mode and SWPE when compared with nonlinear-mode results for the 1:8 spheroid.

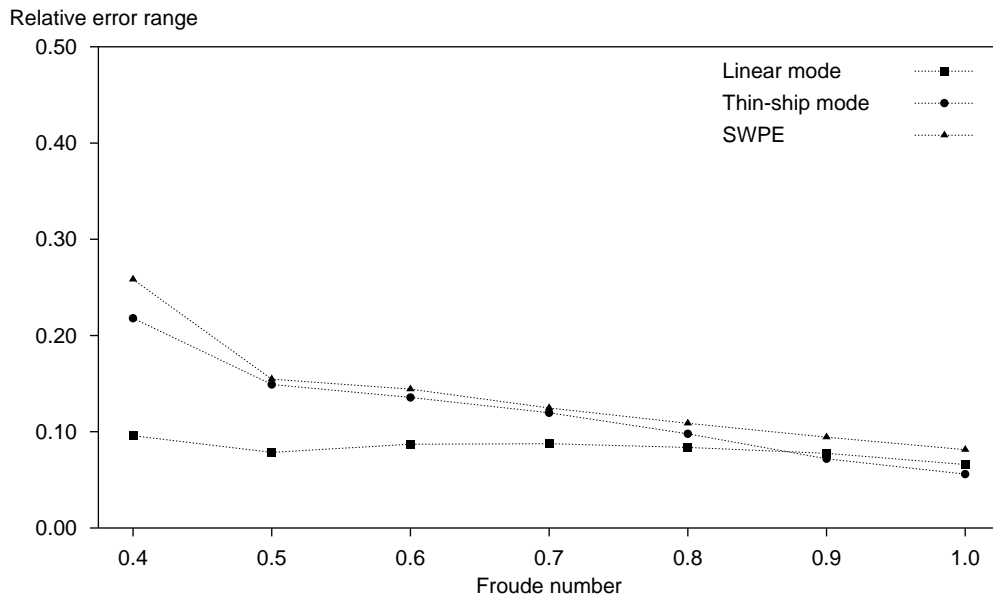


Figure 16: Relative error range in the free surface as produced by linear mode, thin-ship mode and SWPE when compared with nonlinear-mode results for the 1:10 spheroid.

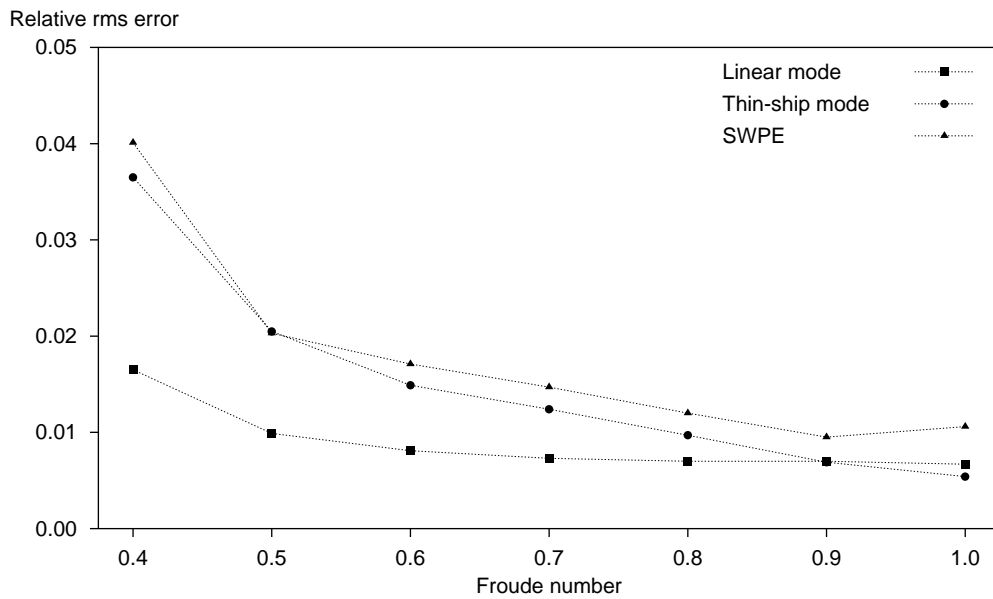


Figure 17: Relative rms error in the free surface as produced by linear mode, thin-ship mode and SWPE when compared with nonlinear-mode results for the 1:10 spheroid.

gravitational acceleration is 9.81 metres per second per second, and the spheroid's length is 100 metres. In general, there is excellent agreement.

At Froude number 0.4, near the left-hand side of the plot there is a small error (of the order of 17% compared with the thin-ship-mode's 12%), which is thought to be due to the inability of the current implementation of SWPE to handle the extreme near field (the stern of the spheroid is at 50 metres, very close to the region where this error occurs). The present version of SWPE is strictly a far-field code, intended for use beyond about one ship's length and one transverse wavelength of the stern. However, it does seem to retain reasonable accuracy closer to the stern. The present contract specifies only far field computations by SWPE. If any extension occurs into 1999-2000, one of the first tasks will be inclusion of near-field effects in SWPE, which will eliminate this particular source of error.

At Froude numbers 0.8 and 1.0, there appears to be a "speckling" within the wake. This is not an error inherent in SWPE, but rather one that manifests itself in the verification code at high Froude number. As the Froude number is increased, the "diverging" waves (those travelling at angles greater than  $35^\circ$  to the direction of the body's motion) become increasingly more energetic and, as the angle of wave propagation tends towards perpendicular to the direction of the vessel's motion (that is, crest lines become tangent to that direction), the local wave-length decreases. It is impossible for any method that uses a discrete representation of the free surface (as does the verification code) to resolve such extremely short waves adequately, and this results in small errors (in this case of the order of 3%) in the free surface. This source of error affects the verification code in all of its modes, and so is not seen when one mode is compared to the other (hence there is no apparent speckling in the lower half of the figure). Rather, since the SWPE computations do not suffer from this defect, they appear as a difference between the verification code's nonlinear result and SWPE's free surface, which manifests itself as speckling in the upper half of the figure. Apparently, at Froude number 0.6, this speckling affects the nonlinear-mode more than it does the thin-ship mode, and so it is seen in both halves of the corresponding figure.

Finally, Figures 22–25 show the actual surfaces obtained by the verification code in nonlinear mode (the lower half of the plots) and the SWPE code (the upper half of the plots) at Froude numbers of 0.4, 0.6, 0.8 and 1.0. One can see, as could have been inferred from the magnitude of the errors in the previous plots, that the agreement is in general very good, with the major source of error being that the waves are slightly smaller in amplitude for the SWPE case, due to its inability to capture the near-nose and tail flow about the submerged spheroid. Upon close inspection, one can see the slight difference in the near field for the case of Froude

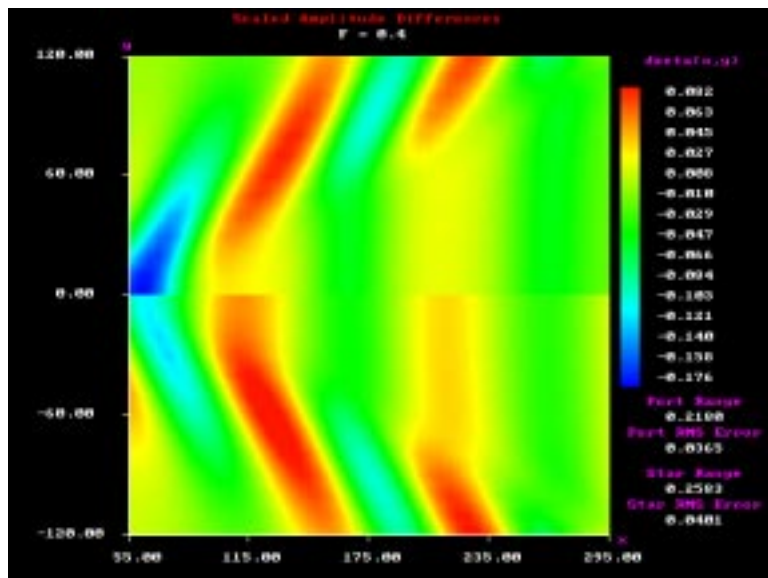


Figure 18: Relative error in the free surfaces produced by SWPE (upper half) and thin-ship mode (lower half) when compared to the nonlinear-mode results for the 1:10 spheroid with diameter-to-depth ratio  $2/3$  at Froude number 0.4.

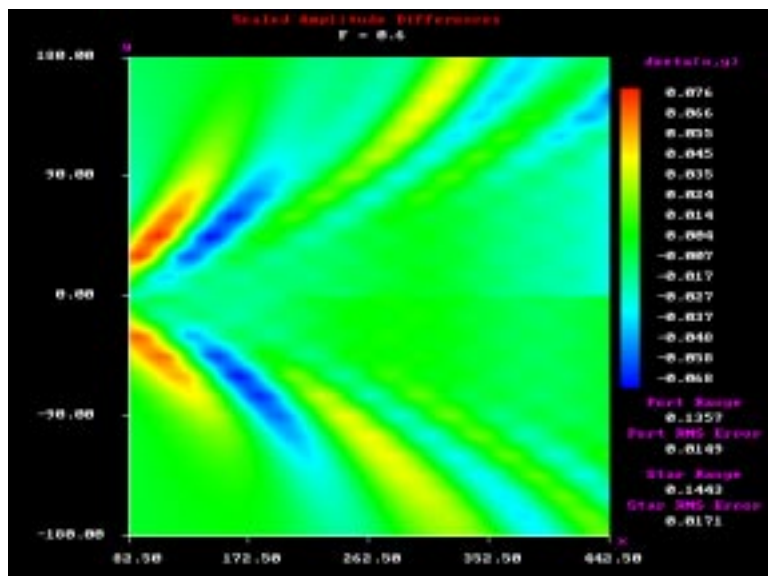


Figure 19: Relative error in the free surfaces produced by SWPE (upper half) and thin-ship mode (lower half) when compared to the nonlinear-mode results for the 1:10 spheroid with diameter-to-depth ratio  $2/3$  at Froude number 0.6.

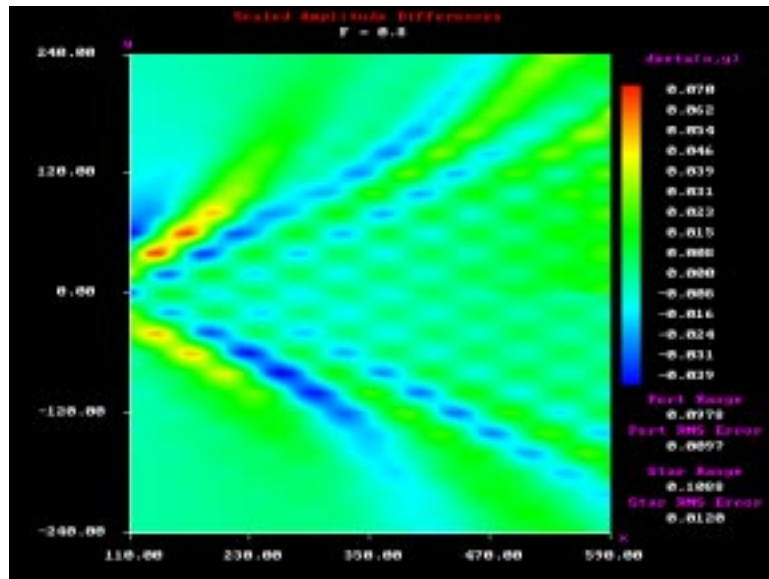


Figure 20: Relative error in the free surfaces produced by SWPE (upper half) and thin-ship mode (lower half) when compared to the nonlinear-mode results for the 1:10 spheroid with diameter-to-depth ratio  $2/3$  at Froude number 0.8.

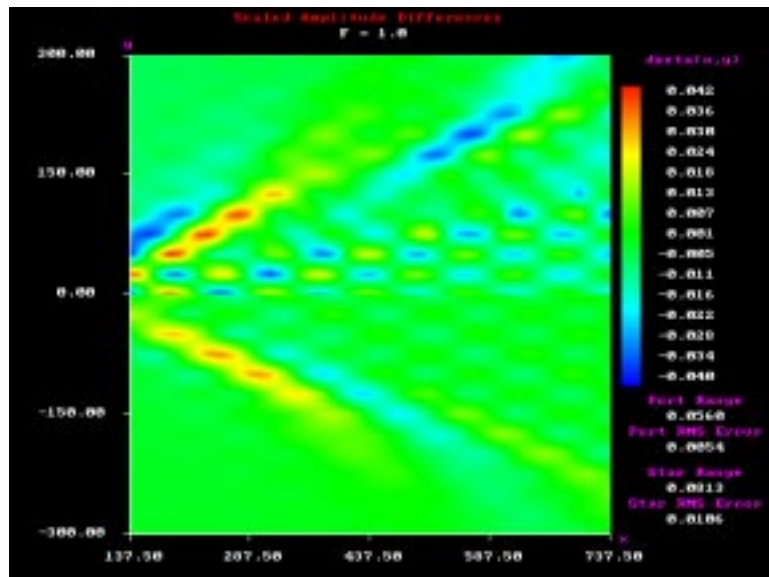


Figure 21: Relative error in the free surfaces produced by SWPE (upper half) and thin-ship mode (lower half) when compared to the nonlinear-mode results for the 1:10 spheroid with diameter-to-depth ratio  $2/3$  at Froude number 1.0.

number 0.4, due to the fact that the present version of SWPE is strictly a far-field implementation.

Under even closer inspection, one can perhaps see striations in the internal region of the wake extending across the major wave crests along the Kelvin angle, for Froude numbers 0.8 and 1.0. This leads to the speckling observed in the error plots of Figures 20–21. As indicated above, this phenomenon is a numerical artefact due to the low resolution of the verification code, and is not present in SWPE when used at adequate resolution. It occurs in the starboard (SWPE) parts of Figures 24–25 only because in those Figures, SWPE is artificially constrained to a low resolution matching that of the verification program.

To illustrate that the speckling effect is not present in SWPE, Figure 26 is a higher resolution version of Figure 24 at Froude number 0.8, both port and starboard sides now being computed by SWPE. No speckling or striations are observable. Incidentally, the front cover of this report contains a far-field version of the same SWPE computations.

In passing, it is interesting to note in Figures 22–25 the dramatic change in the character of the wake as the Froude number increases, with mostly “transverse” waves at Froude number 0.4, but mostly “diverging” waves at Froude number 1.0.

## 4 Conclusion

We have considered the flow about a spheroid submerged beneath a free surface and subject to different assumptions, namely the thin-ship theory, the linearised free-surface boundary condition, and the fully-nonlinear approach. Specifically, we have considered spheroids of diameter-to-length ratios 1:8 and 1:10, over the range of length-based Froude numbers 0.3–1.0, and diameter-to-depth ratios 0.1–1.0.

We have, by comparing with the analytic expression derived by Havelock using slender-body theory, shown that the representation of the free-surface and body used in the linear and nonlinear mode calculations is adequate to provide accurate results.

We have determined the error which is inherent in the thin-ship theory in comparison to the nonlinear theory, and we have considered, by implementing the linearised free-surface boundary condition while satisfying the Neumann boundary condition on the body, the separate effects of the thin-ship theory approximations, namely the linearised free-surface boundary condition and the representation of the body by a distribution of singularities along the centre plane. In doing so, we

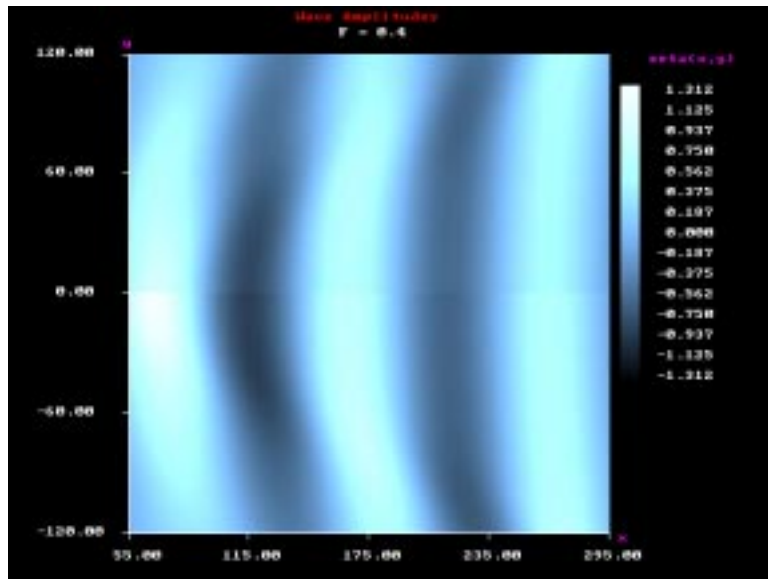


Figure 22: Free surfaces produced by SWPE (upper half) and nonlinear mode (lower half) for the 1:10 spheroid with diameter-to-depth ratio  $2/3$  at Froude number 0.4.

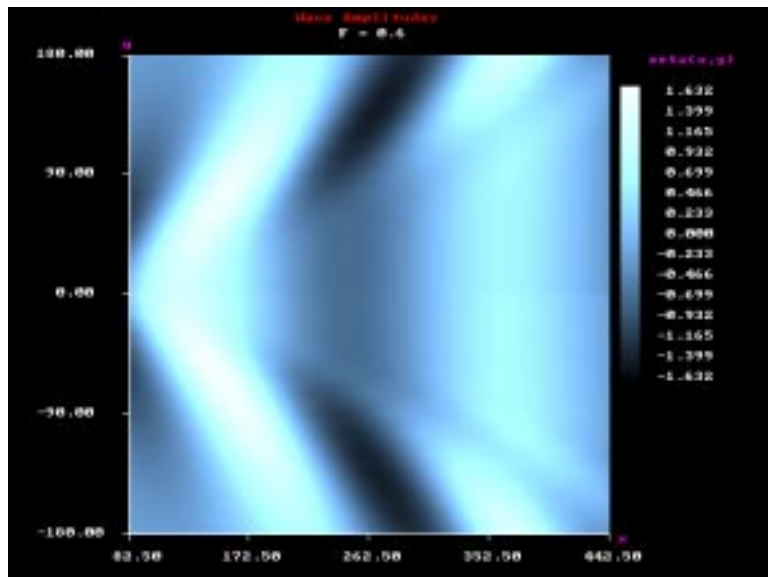


Figure 23: Free surfaces produced by SWPE (upper half) and nonlinear mode (lower half) for the 1:10 spheroid with diameter-to-depth ratio  $2/3$  at Froude number 0.6.

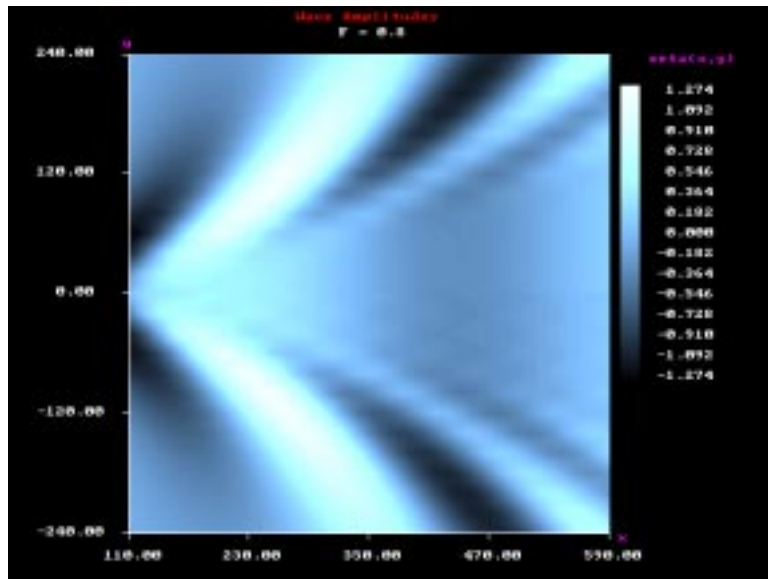


Figure 24: Free surfaces produced by SWPE (upper half) and nonlinear mode (lower half) for the 1:10 spheroid with diameter-to-depth ratio  $2/3$  at Froude number 0.8.

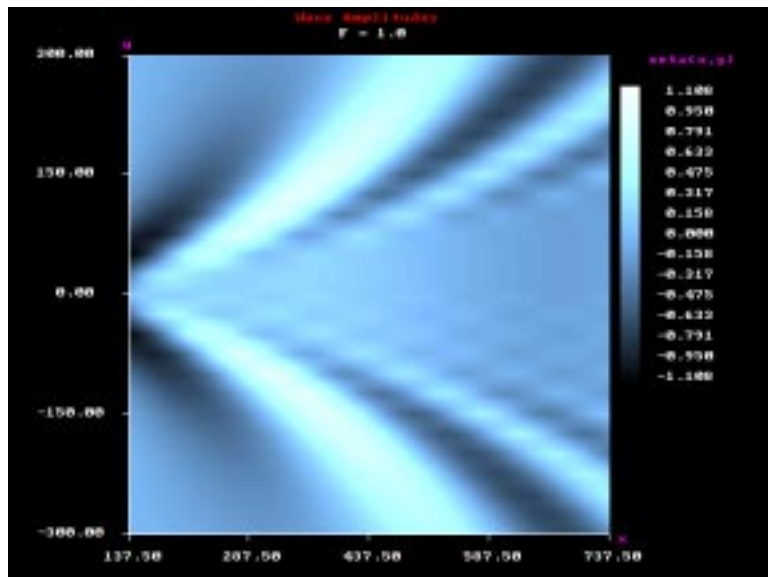


Figure 25: Free surfaces produced by SWPE (upper half) and nonlinear mode (lower half) for the 1:10 spheroid with diameter-to-depth ratio  $2/3$  at Froude number 1.0.

have found that there is an error due to the body representation that is present in all thin-ship results, which allows a small volume of fluid to enter the body near the bow and exit the body near the stern, the effect of which is to under-represent the body, resulting in a smaller disturbance to the flow, and hence the free surface, than would otherwise be expected. We have confirmed that the effect of the linearised free-surface boundary condition is negligible at very deep submergences, with its effect becoming increasingly important as the depth of the spheroid is decreased.

Finally, we have compared, for the diameter-to-depth ratio of  $2/3$ , the results produced in linear mode, thin-ship mode and by SWPE with the nonlinear-mode results. Although there exists a small non-reducible error due to the representation of the body under thin-ship theory, it is felt that the quality of the results created by SWPE is sufficient. This is an important conclusion, given the speed with which the latter can be computed.

## References

- [1] T.H. Havelock, *The wave resistance of a spheroid*, Proceedings of the Royal Society of London, Ser. A **131** (1931), 275–285.
- [2] D.C. Scullen, *Accurate computation of steady nonlinear free-surface flows*, Ph.D. thesis, Department of Applied Mathematics, The University of Adelaide, February 1998.
- [3] D.C. Scullen and E.O. Tuck, *Nonlinear free-surface flow computations for submerged cylinders*, Journal of Ship Research **39** (1995), 185–193.
- [4] E.O. Tuck, *The effect of non-linearity at the free surface on flow past a submerged cylinder*, Journal of Fluid Mechanics **22** (1965), 401–414.
- [5] E.O. Tuck, L. Lazauskas, and D.C. Scullen, *Sea wave pattern evaluation part 1 report: Primary code and test results (surface vessels)*, Internal report (1999).

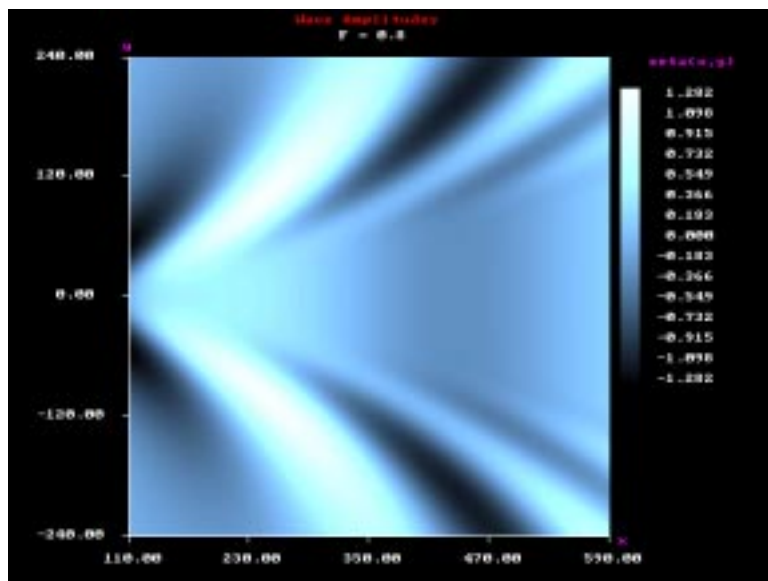


Figure 26: Free surfaces produced by SWPE (symmetric top and bottom) at high resolution (300 by 300 grid) for the 1:10 spheroid with diameter-to-depth ratio  $2/3$  at Froude number 0.8.